Metrology of the Aether Unit and Curl in QMU: Operational Extraction of A_u and Non-Circular Ledger Tests with Defined Curl and Cavity-Perturbation Derivation

David W. Thomson
Quantum AetherDynamics Institute

October 27, 2025

Abstract

We present an operational metrology to extract the aether unit A_u from three blueprint experiments—(i) an Aharonov–Bohm (AB)–type interferometer with engineered aetheric phase bias, (ii) a tunable cavity perturbed by structured boundaries, and (iii) a Casimir-configured insert serving as a QMU boundary-control differential—using only Quantum Measurement Units (QMU). In parallel we obtain an independent electrostatic estimate $\widehat{k_C}$. Treating the curl as a defined ledger constant $\mathrm{curl}_{\mathrm{def}} \equiv {e_{\mathrm{emax}}}^2/(m_e\lambda_C)$, the experimental couplings are strictly dimensionless via the factor

$$\Gamma_Q \equiv \frac{A_u\,\mathrm{curl}_{\mathrm{def}}}{{F_q}^2{\lambda_C}^2}.$$

We perform two non-circular ledger tests:

$$\text{(Ratio)}\quad A_u/k_C = 16\pi^2, \qquad \text{(Triad)}\quad A_u\,\mathrm{curl}_{\mathrm{def}} = {F_q}^2{\lambda_C}^2.$$

A QMU-native cavity-perturbation derivation (Slater/Bethe–Schwinger lineage) yields a dimensionless boundary functional $\mathcal{C}(\alpha)$ and a practical workflow to compute coefficients c_1, c_2 from $\mathcal{C}(\alpha) = c_1\alpha^{-1} + c_2\alpha^{-2} + O(\alpha^{-3})$. Interferometer and cavity paths provide $\widehat{A_u}$ estimators that combine via BLUE with correlated uncertainties from the shared (F_q, λ_C) realizations. Successful closure elevates A_u to a primary operational quantity in QMU and validates the aether–electromagnetic–kinematic ledger across independent apparatus classes.

Contents

1 Operational Frame and Hypotheses (QMU) 2

2 Interferometer Protocol (AB-type with Duality Bias) 3
2.1 Geometry and response . . . 3
2.2 Measuring $\mathcal{J}$ . . . 3
2.3 Estimator and uncertainty . . . 3
2.4 Minimal schematic . . . 4

3 Cavity Protocol with Boundary Control 4
3.1 Frequency pull and common ratio . . . 4
3.2 Estimators . . . 4

4 Joint Inference and Correlated Uncertainty **5**
4.1 Consensus $\widehat{A_u}$ 5

5 Ledger Tests and Validation Tiers **5**

6 Uncertainty, Systematics, and Mitigations **6**
6.1 Budget template (QMU-only) 6

7 Electrostatic Path for k_C and Ratio Test **7**

8 Implementation: Standards, Fixtures, and Templates **7**
8.1 QMU standards 7
8.2 Bill of materials (dimensionless ledger) 7
8.3 Data templates 8

9 Verification Pathways and Discovery Opportunities **8**

10 Conclusions **8**

A Ledger: Definitions and Identities Under Test **8**

B Geometry Functionals and Worked Examples **9**
B.1 Interferometer functional $\mathcal{J}$ 9
B.2 Cavity perturbation in QMU and computing c_1, c_2 9

C Uncertainty Propagation and Correlations **10**

D Electrostatic Path Scaling for k_C **10**

E Data-Reduction Worksheet (Worked Symbolic Example) **10**

1 Operational Frame and Hypotheses (QMU)

All measurements and reported quantities are in QMU [17]. Observables enter as dimensionless ratios and phases. Whenever a frequency appears, it is normalized by F_q; whenever a length appears, it is normalized by λ_C. Thus, the only admissible dimensionful symbols in the main text are the ledger bases ($m_\mathrm{e}, \lambda_C, F_q, e^2, {e_\mathrm{emax}}^2$); derived QMU (e.g., volm $= {\lambda_C}^3$, rson $= {F_q}^2$, mflx $= m_\mathrm{e}{\lambda_C}^2 F_q/{e_\mathrm{emax}}^2$) are cataloged in Appendix A.

Aether unit A_u. Operational target of this metrology: a scaling constant that couples geometric functionals to phase/frequency pulls in AB-type and cavity experiments under QMU normalization. The AB pathway leverages phase sensitivity to enclosed flux and topology [1–3].

Electrostatic constant k_C. Electrostatic path target (QMU): measured via balanced-geometry energy comparisons that yield a dimensionless ratio proportional to k_C (Appendix D).

Defined ledger constant. We *define* the curl quantity

$$\mathrm{curl}_{\mathrm{def}} \equiv \frac{{e_{\mathrm{emax}}}^2}{m_{\mathrm{e}}\,\lambda_C}. \tag{1}$$

It is not extracted from data in this work.

Hypotheses under test. The experimental program targets two APM/QMU ledger identities [18]:

$$\text{(H1: ratio)}\quad \frac{A_u}{k_C} = 16\pi^2, \qquad \text{(H2: triad)}\quad A_u\,\mathrm{curl}_{\mathrm{def}} = {F_q}^2{\lambda_C}^2. \tag{2}$$

Metrology objective. Estimate A_u from independent, redundantly constrained experiments and estimate k_C from an electrostatic path; then test (2) via residuals relative to predeclared QMU tolerances.

2 Interferometer Protocol (AB-type with Duality Bias)

2.1 Geometry and response

Consider a two-path interferometer whose differential path couples to aetheric structure via a winding functional $\mathcal{J}$ (purely geometric, QMU-normalized). The predicted phase pull is

$$\Delta\phi = \mathcal{J}\,\frac{A_u\,\mathrm{curl}_{\mathrm{def}}}{{F_q}^2{\lambda_C}^2}, \qquad \Rightarrow \quad \mathcal{R}_1 \equiv \frac{\Delta\phi}{\mathcal{J}} = \frac{A_u\,\mathrm{curl}_{\mathrm{def}}}{{F_q}^2{\lambda_C}^2}. \tag{3}$$

Here $\mathcal{J}$ encodes loop linking number, directed area in ${\lambda_C}^2$ units, path-twist parity, and any engineered duality bias. *Duality bias:* introduce a path element (e.g., chiral scatterers or structured boundaries) whose parity flip $\chi \in \{\pm 1\}$ toggles the sign component embedded in $\mathcal{J}$, separating aetheric phase from electromagnetic backgrounds by differencing $\chi = \pm 1$ shots [4–7].

2.2 Measuring $\mathcal{J}$

Parameterize $\mathcal{J} = \nu\,\sigma\,\chi$ with integer windings ν, directed area σ in ${\lambda_C}^2$ units, and parity χ. The area σ is determined from CAD geometry in λ_C-normalized coordinates; ν is set by loop design and verified by imaging; χ is controlled via a reversible insert.

2.3 Estimator and uncertainty

Given N phase shots $\{\Delta\phi_i\}$ with known $\{\mathcal{J}_i\}$,

$$\widehat{A_u}^{(1)} = \frac{{F_q}^2{\lambda_C}^2}{\mathrm{curl}_{\mathrm{def}}}\,\frac{\sum_i w_i\,\Delta\phi_i/\mathcal{J}_i}{\sum_i w_i}, \qquad w_i = \frac{1}{u^2(\Delta\phi_i) + \Delta\phi_i^2\,u^2(\mathcal{J}_i)/\mathcal{J}_i^2}. \tag{4}$$

The corresponding standard uncertainty is

$$u^2\!\left(\widehat{A_u}^{(1)}\right) = \left(\frac{{F_q}^2{\lambda_C}^2}{\mathrm{curl}_{\mathrm{def}}}\right)^2 \left(\sum_i w_i\right)^{-1}. \tag{5}$$

Uncertainty evaluation follows GUM principles (adapted to QMU realizations) [16].

2.4 Minimal schematic

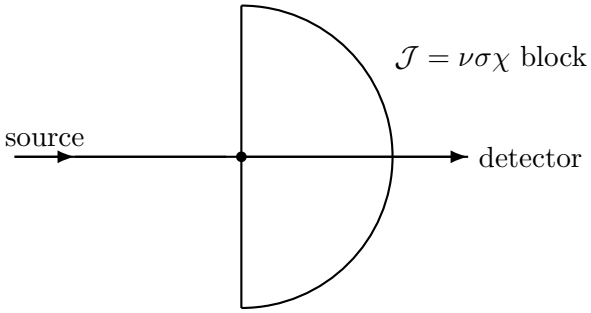

Figure 1: AB-type interferometer with parity-toggling duality bias inside the structured region.

3 Cavity Protocol with Boundary Control

3.1 Frequency pull and common ratio

Let $a = \alpha\,\lambda_C$ be the boundary separation in QMU. The cavity mode frequency f (normalized by F_q) experiences a relative pull

$$\frac{\Delta f}{f} = \mathcal{C}(\alpha)\,\frac{A_u\,\mathrm{curl}_{\mathrm{def}}}{{F_q}^2{\lambda_C}^2}, \qquad \Rightarrow \quad \mathcal{R}_2 \equiv \frac{\Delta f}{f\,\mathcal{C}(\alpha)} = \frac{A_u\,\mathrm{curl}_{\mathrm{def}}}{{F_q}^2{\lambda_C}^2}, \tag{6}$$

where $\mathcal{C}(\alpha)$ is a precomputed, dimensionless boundary functional (Appendix B). The small-perturbation treatment follows the Slater/Bethe–Schwinger cavity framework [10–13] (rendered in QMU) [14].

Introduce a removable Casimir-configured [8, 9] insert that modifies $\mathcal{C}(\alpha) \mapsto \mathcal{C}(\alpha) + \delta\mathcal{C}$. The differential ratio

$$\Delta\!\left(\frac{\Delta f}{f}\right) = \delta\mathcal{C}\,\frac{A_u\,\mathrm{curl}_{\mathrm{def}}}{{F_q}^2{\lambda_C}^2} \quad \Rightarrow \quad \mathcal{R}_3 \equiv \frac{\Delta(\Delta f/f)}{\delta\mathcal{C}} = \frac{A_u\,\mathrm{curl}_{\mathrm{def}}}{{F_q}^2{\lambda_C}^2}. \tag{7}$$

Thus $\mathcal{R}_1 = \mathcal{R}_2 = \mathcal{R}_3$ by construction, providing an internal redundancy check.

3.2 Estimators

Given M measurements at $\{\alpha_j\}$:

$$\widehat{A_u}^{(2)} = \frac{{F_q}^2{\lambda_C}^2}{\mathrm{curl}_{\mathrm{def}}}\,\frac{\sum_j v_j\,\frac{\Delta f_j}{f_j\,\mathcal{C}(\alpha_j)}}{\sum_j v_j}, \quad v_j = \left[u^2\!\left(\frac{\Delta f_j}{f_j\,\mathcal{C}(\alpha_j)}\right)\right]^{-1}. \tag{8}$$

For differential insert toggles (this is $\widehat{A_u}^{(3)}$):

$$\widehat{A_u}^{(3)} = \frac{{F_q}^2{\lambda_C}^2}{\mathrm{curl}_{\mathrm{def}}}\,\frac{\Delta(\Delta f/f)}{\delta\mathcal{C}}. \tag{9}$$

The $\widehat{A_u}^{(3)}$ path cancels common-mode readout drifts and isolates boundary-functional uncertainty.

4 Joint Inference and Correlated Uncertainty

4.1 Consensus $\widehat{A_u}$

Collect $\widehat{A_u}^{(k)}$ (with $k = 1, 2, 3$). Let $\widehat{\boldsymbol{A}} = (\widehat{A_u}^{(1)}, \widehat{A_u}^{(2)}, \widehat{A_u}^{(3)})^\top$ and covariance matrix $\boldsymbol{\Sigma}$ which includes *shared* realization uncertainties for F_q and λ_C. The best linear unbiased estimate (BLUE; Gauss–Markov/Aitken) [15] is

$$\widehat{A_u} = \frac{\mathbf{1}^\top \boldsymbol{\Sigma}^{-1} \widehat{\boldsymbol{A}}}{\mathbf{1}^\top \boldsymbol{\Sigma}^{-1} \mathbf{1}}, \qquad u^2(\widehat{A_u}) = \frac{1}{\mathbf{1}^\top \boldsymbol{\Sigma}^{-1} \mathbf{1}}. \tag{10}$$

Here $\boldsymbol{\Sigma}$ has diagonal elements from path-specific noise (Type A, and Type B from $\mathcal{J}$ or $\mathcal{C}$) and off-diagonals from common standards:

$$\mathrm{Cov}\left(\widehat{A_u}^{(k)}, \widehat{A_u}^{(l)}\right) \supset \left(\frac{{F_q}^2 {\lambda_C}^2}{\mathrm{curl}_{\mathrm{def}}}\right)^2 \left[\left(\frac{u(F_q)}{F_q}\right)^2 + \left(\frac{u(\lambda_C)}{\lambda_C}\right)^2\right], \quad k \neq l. \tag{11}$$

Uncertainty combination and reporting follow GUM conventions for realizations [16].

5 Ledger Tests and Validation Tiers

With the consensus $\widehat{A_u}$ (Sec. 4), the electrostatic measurement $\widehat{k_C}$ (Sec. 7), and the defined $\mathrm{curl}_{\mathrm{def}}$ in (1), we test the two ledger hypotheses (2).

Ratio Test (H1).

$$\frac{\widehat{A_u}}{\widehat{k_C}} \stackrel{?}{=} 16\pi^2, \qquad \text{residual } \delta_{A/k} = \frac{\widehat{A_u}}{\widehat{k_C}} - 16\pi^2. \tag{12}$$

Triad Product Test (H2).

$$\delta_\times \equiv \frac{\widehat{A_u}\ \mathrm{curl}_{\mathrm{def}}}{{F_q}^2 {\lambda_C}^2} - 1. \tag{13}$$

Validation tiers (predeclared tolerances). Both residuals $\delta_{A/k}$ and $\delta_\times$ are evaluated against predeclared tolerances τ_1, τ_2.

Table 1: Example validation tiers.

Tier	τ_1 for $\lvert\delta_{A/k}\rvert$	τ_2 for $\lvert\delta_\times\rvert$
Pilot	10^{-3}	10^{-3}
Baseline	10^{-4}	10^{-4}
Flagship	10^{-5}	10^{-5}

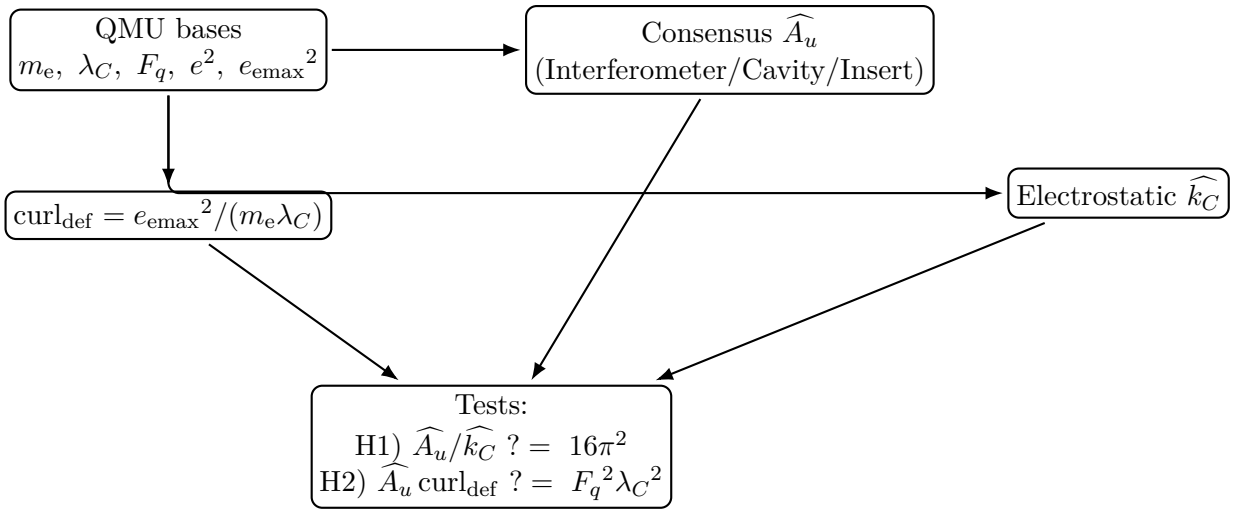

Figure 2: Non-circular verification flow. curl is defined from QMU bases; A_u and k_C are independently measured. Two identities are then tested.

6 Uncertainty, Systematics, and Mitigations

Dominant sources. (i) Geometric functionals $\mathcal{J}$ and $\mathcal{C}$; (ii) phase readout nonlinearity; (iii) cavity frequency drift; (iv) insert positioning repeatability; (v) realization of the timing base used to normalize to F_q; (vi) realization of the length base used to normalize to λ_C; (vii) path parity and winding miscounts.

Standards versus realizations. In QMU, F_q and λ_C are defined ledger bases. Uncertainties $u(F_q)$ and $u(\lambda_C)$ appearing below refer to the *experimental realizations* of those references (e.g., timing-chain and geometric-traceability chains), not uncertainties in their definitions.

6.1 Budget template (QMU-only)

Table 2: Illustrative standard-uncertainty budget (relative, all QMU).

Contributor	Symbol	Rel. std. unc.	Type
Phase readout	$u(\Delta\phi)/\Delta\phi$	u_ϕ	A
Interferometer geometry	$u(\mathcal{J})/\mathcal{J}$	u_J	B
Cavity pull metrology	$u(\Delta f/f)/(\Delta f/f)$	u_f	A
Boundary functional	$u(\mathcal{C})/\mathcal{C}$	u_C	B
Insert repeatability	$u(\delta\mathcal{C})/\delta\mathcal{C}$	$u_{\delta C}$	B
Timing base realization	$u(F_q)/F_q$	u_{F_q}	B
Compton scaling realization	$u(\lambda_C)/\lambda_C$	u_{λ_C}	B
Combined (phase path)		$\sqrt{u_\phi^2 + u_J^2 + u_{F_q}^2 + u_{\lambda_C}^2}$	
Combined (cavity path)		$\sqrt{u_f^2 + u_C^2 + u_{F_q}^2 + u_{\lambda_C}^2}$	

7 Electrostatic Path for k_C and Ratio Test

We implement an electrostatic energy comparison in QMU to obtain $\widehat{k_C}$ without SI detours. The apparatus compares a calibrated charge configuration (charges expressed via e^2 and ${e_{\text{emax}}}^2$ scaling) against an interferometric reference, producing a dimensionless ratio proportional to k_C. A balanced geometry (Fig. 3) compares two QMU-scaled configurations whose energy difference is

$$\Delta U = k_C \, G_{\text{geom}}, \tag{14}$$

with G_{geom} a pure number computed from the chosen layout in λ_C-normalized coordinates (Appendix D). Measuring $\Delta U / G_{\text{geom}}$ yields $\widehat{k_C}$; sweeping the geometry overdetermines G_{geom} and isolates systematics. The concluding ratio test is (12).

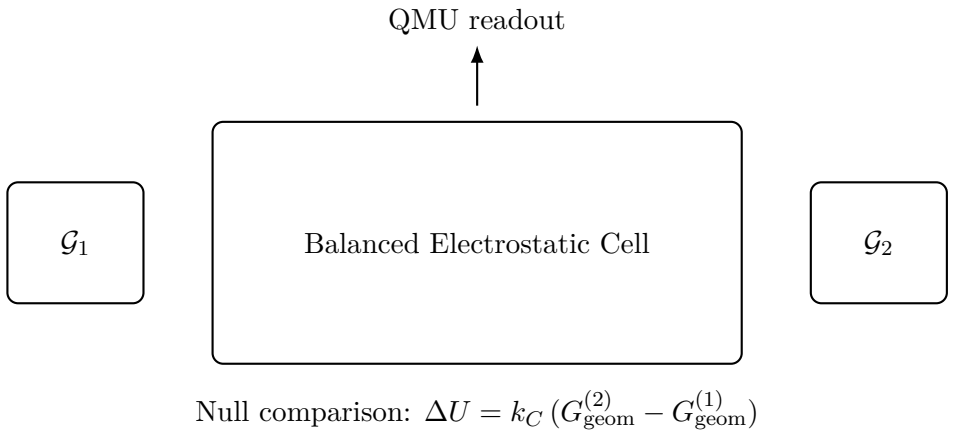

Figure 3: Minimal balanced geometry for $\widehat{k_C}$: two QMU-scaled configurations $\mathcal{G}_1, \mathcal{G}_2$ yield a dimensionless energy difference.

8 Implementation: Standards, Fixtures, and Templates

8.1 QMU standards

- **Frequency base:** normalize all frequency readouts to F_q (ledger); plots and regressions use F_q ratios.
- **Length base:** all physical lengths are recorded as multiples of λ_C.
- **Charge base:** use e^2 and ${e_{\text{emax}}}^2$ for scaling of electrostatic or magnetic boundary couplings.

8.2 Bill of materials (dimensionless ledger)

Subsystem	Ledger parameter	Control
Interferometer arms	$\mathcal{J} = \nu\sigma\chi$	Parity flips, loop count scans
Cavity boundaries	$\mathcal{C}(\alpha)$	α sweep in λ_C units
Insert module	$\delta\mathcal{C}$	in/out toggles, hysteresis check
Timing base	F_q	beat comparison to realization chain

Compton scaling	λ_C	geometric calibration tree
Electrostatic path	k_C	null test via balanced geometry

8.3 Data templates

Table 4: Interferometer shots (all QMU).

i	$\Delta\phi_i$	$\mathcal{J}_i$	$\Delta\phi_i/\mathcal{J}_i$	$u(\Delta\phi_i/\mathcal{J}_i)$
(to be filled during experiment)				

Table 5: Cavity pulls at α_j (all QMU).

j	α_j	$\Delta f_j/f_j$	$\mathcal{C}(\alpha_j)$	Ratio	Std. unc.
(to be filled during experiment)					

9 Verification Pathways and Discovery Opportunities

Ledger correlations. Successful ratio and triad tests operationally correlate $(\widehat{A_u}, \widehat{k_C})$ with the defined bases $(F_q, \lambda_C, m_\mathrm{e}, {e_\mathrm{emax}}^2)$ through pure-number identities. Because $16\pi^2$ is topological in the ledger, empirical confirmation in metrology constitutes a stringent test of QMU structure.

Redundancy map. Because $\mathcal{R}_1 = \mathcal{R}_2 = \mathcal{R}_3$, internal incoherence among the three paths diagnoses geometry or readout systematics independently of the ledger tests.

Sensitivity studies. By scanning α (cavity) and loop parity (interferometer), one can map response linearity in the small-pull regime and search for regulated departures that may indicate higher-order QMU corrections. Any systematic drift tracking mflx-weighted combinations is an explicit target for refinement.

10 Conclusions

We provided three independent, QMU-pure methods to estimate A_u, an electrostatic method to estimate k_C, and two non-circular ledger tests: the aether–electrostatic ratio and the triad product using the *defined* $\mathrm{curl}_\mathrm{def} = {e_\mathrm{emax}}^2/(m_\mathrm{e}\lambda_C)$. The design emphasizes (i) geometric functionals computable in QMU, (ii) cross-ratio estimators that cancel drifts, (iii) an explicit distinction between standards and their realizations with correlated-uncertainty handling, and (iv) declared ledger-closure tolerances. A successful run upgrades A_u to a primary operational quantity and validates the APM/QMU bridge across aetheric, electromagnetic, and kinematic scales.

A Ledger: Definitions and Identities Under Test

Definitions (QMU).

$$\mathrm{curl}_\mathrm{def} = \frac{{e_\mathrm{emax}}^2}{m_\mathrm{e}\lambda_C}, \qquad \mathrm{mflx} = \frac{m_\mathrm{e}{\lambda_C}^2 F_q}{{e_\mathrm{emax}}^2}, \qquad \mathrm{rson} = {F_q}^2, \qquad \mathrm{volm} = {\lambda_C}^3. \tag{15}$$

Hypotheses (tested in the main text).

$$\frac{A_u}{k_C} = 16\pi^2, \qquad A_u \,\mathrm{curl}_{\mathrm{def}} = {F_q}^2 {\lambda_C}^2. \tag{16}$$

B Geometry Functionals and Worked Examples

B.1 Interferometer functional $\mathcal{J}$

A convenient parametrization is $\mathcal{J} = \nu\,\sigma\,\chi$, with $\nu \in \mathbb{Z}$ (directed windings), σ (dimensionless area in ${\lambda_C}^2$ units), and $\chi \in \{\pm 1\}$ (parity under duality bias). Each factor is controllable and measurable in QMU [1–3].

B.2 Cavity perturbation in QMU and computing c_1, c_2

Let the unperturbed cavity eigenproblem be posed on the dimensionless domain

$$\mathbf{r}' = \mathbf{r}/\lambda_C, \qquad \nabla' = \lambda_C\,\nabla, \qquad t' = F_q\,t,$$

with modal fields normalized so that the dimensionless energy functional is

$$\mathcal{U} = \frac{1}{2}\int_{\Omega(\alpha)} (\|\boldsymbol{\mathcal{E}}\|^2 + \|\boldsymbol{\mathcal{B}}\|^2)\,\mathrm{d}^3\mathbf{r}',$$

and boundary separation $a = \alpha\,\lambda_C$. A small boundary deformation $\alpha \mapsto \alpha + \delta\alpha$ induces a first-order fractional frequency shift

$$\frac{\Delta f}{f} = \underbrace{\left[\frac{\displaystyle\int_{\partial\Omega}\left(\eta_E\,\|\boldsymbol{\mathcal{E}}_{\parallel}\|^2 - \eta_B\,\|\boldsymbol{\mathcal{B}}_{\perp}\|^2\right)\delta n'\,\mathrm{d}S'}{\displaystyle\int_{\Omega}(\|\boldsymbol{\mathcal{E}}\|^2 + \|\boldsymbol{\mathcal{B}}\|^2)\,\mathrm{d}^3\mathbf{r}'}\right]}_{\mathcal{C}(\alpha)} \times \frac{A_u\,\mathrm{curl}_{\mathrm{def}}}{{F_q}^2{\lambda_C}^2}. \tag{17}$$

Here $\delta n'$ is the dimensionless normal displacement, η_E, η_B are pure-number coefficients fixed by the boundary condition class, and all fields are the dimensionless eigenfields on $\Omega(\alpha)$ [10–14]. For many common symmetries,

$$\mathcal{C}(\alpha) = c_1\alpha^{-p} + c_2\alpha^{-p-1} + O(\alpha^{-p-2}), \qquad p > 0.$$

Analytic example (parallel plates, PEC, lowest mode). Consider a 1D symmetric cavity with perfectly conducting plates at $z' = 0$ and $z' = \alpha$, uniform displacement $\delta n' = \delta\alpha$. For the fundamental mode with frequency $f \propto \alpha^{-1}$, one has

$$\frac{\Delta f}{f} = -\,\frac{\delta\alpha}{\alpha}.$$

Comparing with (17) (uniform $\delta n'$ and normalized denominator) gives

$$\mathcal{C}(\alpha) = -\,\alpha^{-1} \quad \Rightarrow \quad c_1 = -1,\ c_2 = 0,\ p = 1.$$

Higher-order geometry corrugations or a structured insert generate the $O(\alpha^{-2})$ correction that populates c_2.

General FEM workflow (dimensionless) to extract c_1, c_2.

1. **Solve the eigenproblem** on $\Omega(\alpha_j)$ for a sweep $\{\alpha_j\}$ (all in QMU units), obtaining $\boldsymbol{\mathcal{E}}_j, \boldsymbol{\mathcal{B}}_j$.
2. **Evaluate** $\mathcal{C}(\alpha_j)$ via (17) using the numerical fields and the chosen boundary displacement pattern $\delta n'$ (e.g., uniform normal shift, patterned insert, etc.). Each $\mathcal{C}(\alpha_j)$ is a pure number.
3. **Fit the model** $\mathcal{C}(\alpha_j) = c_1\alpha_j^{-1} + c_2\alpha_j^{-2}$ by weighted least squares. Let

$$y_j = \mathcal{C}(\alpha_j), \quad X_j = \begin{bmatrix}\alpha_j^{-1} & \alpha_j^{-2}\end{bmatrix}, \quad \mathbf{X} = \begin{bmatrix}X_1 \\ \vdots \\ X_M\end{bmatrix}, \quad \mathbf{y} = \begin{bmatrix}y_1 \\ \vdots \\ y_M\end{bmatrix}.$$

   With weight matrix $\mathbf{W} = \mathrm{diag}(w_j)$, $w_j = 1/u^2(y_j)$,

$$\begin{bmatrix}\widehat{c}_1 \\ \widehat{c}_2\end{bmatrix} = (\mathbf{X}^\top\mathbf{W}\mathbf{X})^{-1}\mathbf{X}^\top\mathbf{W}\mathbf{y}, \quad \mathrm{Cov}(\widehat{c}_1, \widehat{c}_2) = (\mathbf{X}^\top\mathbf{W}\mathbf{X})^{-1}.$$

4. **Use** $\widehat{c}_1, \widehat{c}_2$ in Eqs. (6)–(7) to form $\widehat{A_u}^{(2)}$ and $\widehat{A_u}^{(3)}$.

This procedure keeps all quantities QMU-pure; any numerical solver needs only α-scaled geometry and dimensionless fields.

C Uncertainty Propagation and Correlations

For the interferometer ratio $r_i = \Delta\phi_i/\mathcal{J}_i$,

$$u^2(r_i) = \left(\frac{1}{\mathcal{J}_i}\right)^2 u^2(\Delta\phi_i) + \left(\frac{\Delta\phi_i}{\mathcal{J}_i^2}\right)^2 u^2(\mathcal{J}_i) - 2\,\frac{\Delta\phi_i}{\mathcal{J}_i^3}\mathrm{Cov}(\Delta\phi_i, \mathcal{J}_i). \tag{18}$$

Common-mode contributions from F_q and λ_C realizations enter all paths multiplicatively and thus populate off-diagonal elements of $\boldsymbol{\Sigma}$ used in Sec. 4.

D Electrostatic Path Scaling for k_C

A balanced geometry compares two QMU-scaled configurations $\mathcal{G}_1, \mathcal{G}_2$ that differ by a pure number $G^{(2)}_{\mathrm{geom}} - G^{(1)}_{\mathrm{geom}}$. The observable null is

$$\Delta U = k_C \left(G^{(2)}_{\mathrm{geom}} - G^{(1)}_{\mathrm{geom}}\right). \tag{19}$$

Measuring $\Delta U/\Delta G_{\mathrm{geom}}$ yields $\widehat{k_C}$. Repeating with variable geometry (e.g., rotating through multiple $\mathcal{G}$ pairs) overdetermines G_{geom} and isolates systematics.

E Data-Reduction Worksheet (Worked Symbolic Example)

Inputs (QMU): $\{\Delta\phi_i, \mathcal{J}_i\}_{i=1}^N$, $\{\Delta f_j/f_j, \alpha_j, \mathcal{C}(\alpha_j)\}_{j=1}^M$, and (optionally) the electrostatic $\widehat{k_C}$.

Steps:

1. Compute $r_i = \Delta\phi_i / \mathcal{J}_i$ and its uncertainty.
2. Compute $s_j = (\Delta f_j / f_j)/\mathcal{C}(\alpha_j)$ and its uncertainty.
3. Obtain $\widehat{A_u}^{(1)} = \dfrac{{F_q}^2 {\lambda_C}^2}{\mathrm{curl}_{\mathrm{def}}}\,\overline{r}$, $\widehat{A_u}^{(2)} = \dfrac{{F_q}^2 {\lambda_C}^2}{\mathrm{curl}_{\mathrm{def}}}\,\overline{s}$, and $\widehat{A_u}^{(3)}$ from (7).
4. Build $\boldsymbol{\Sigma}$ including shared realizations of F_q and λ_C; compute consensus $\widehat{A_u}$ (Sec. 4).
5. Obtain $\widehat{k_C}$ via Appendix D.
6. Evaluate $\delta_{A/k}$ and $\delta_{\times}$ (Sec. 5) against tolerances τ_1, τ_2.

References

[1] Y. Aharonov and D. Bohm, Significance of electromagnetic potentials in the quantum theory. *Phys. Rev.* **115**, 485–491 (1959).

[2] A. Tonomura et al., Observation of Aharonov–Bohm effect by electron holography. *Phys. Rev. Lett.* **48**, 1443–1446 (1982).

[3] A. Tonomura et al., Evidence for Aharonov–Bohm effect with magnetic field completely shielded from electron wave. *Phys. Rev. Lett.* **56**, 792–795 (1986).

[4] E. Efrati and W. T. M. Irvine, Orientation-dependent handedness and chiral design. *Phys. Rev. X* **4**, 011003 (2014).

[5] S. J. Yoo and Q. H. Park, Metamaterials and chiral sensing: a review of fundamentals and applications. *Nanophotonics* **8**(7), 1043–1068 (2019).

[6] L. Kang et al., Handedness dependent electromagnetically induced transparency in hybrid chiral metamaterials. *Sci. Rep.* **5**, 10824 (2015).

[7] X. Sha et al., Chirality tuning and reversing with resonant phase-change metasurfaces. *Nat. Commun.* **15**, 2625 (2024).

[8] H. B. G. Casimir, On the attraction between two perfectly conducting plates. *Proc. K. Ned. Akad. Wet.* **51**, 793–795 (1948).

[9] S. K. Lamoreaux, Demonstration of the Casimir force in the 0.6 to 6 μm range. *Phys. Rev. Lett.* **78**, 5–8 (1997). doi:10.1103/PhysRevLett.78.5.

[10] H. A. Bethe, *Theory of Diffraction by Small Holes*, Physical Review 66(7-8), 163–182 (1944).

[11] L. C. Maier Jr. and J. C. Slater, Field strength measurements within a large resonant cavity by the perturbation method. *J. Appl. Phys.* **23**, 68–77 (1952).

[12] E. G. Spencer, Note on cavity perturbation theory. *J. Appl. Phys.* **28**, 130–132 (1957).

[13] R. A. Waldron, Perturbation theory of resonant cavities. *Proc. IEE Part C* **107**, 272–274 (1960).

[14] V. V. Dodonov and A. V. Dodonov, Approximate formulas for the resonance frequency shift in electromagnetic cavities. *Phys. Rev. A* **82**, 043808 (2010).

[15] A. C. Aitken, On least squares and linear combination of observations. *Proc. Roy. Soc. Edinburgh* **55**, 42–48 (1935). (GLS/BLUE).

[16] JCGM 100:2008(E), *Evaluation of Measurement Data — Guide to the Expression of Uncertainty in Measurement (GUM).* Joint Committee for Guides in Metrology (2008). doi:10.59161/JCGM100-2008E.

[17] David W. Thomson III, *Quantum Measurement Units (QMU): A System Based on Quantum Constants and Distributed Charge Geometry.* ResearchGate Preprint (2024). doi:10.13140/RG.2.2.16468.21125.

[18] David W. Thomson III, *[Topological Uniqueness of $A_u/k_C = 16\pi^2$ in the Aether Physics Model (QMU)].* Zenodo (2025). doi:10.5281/zenodo.17336681.